

# Exploring critical behavioral differences in physical, structural, and nuclear radiation attenuation properties of produced High Entropy Alloy (HEA) and Refractory-High Entropy Alloy (RHEA) samples

Seval Hale Güler <sup>a</sup>, Ömer Güler <sup>a</sup>, E. Kavaz <sup>b</sup>, Ghada Almisned <sup>c</sup>, Bashar Issa <sup>d,e</sup>, H.O. Tekin <sup>d,f,\*</sup>

<sup>a</sup> Munzur University, Rare Earth Elements Application and Research Center, 62000, Tunceli, Turkey

<sup>b</sup> Ataturk University, Faculty of Science, Department of Physics, 25240, Erzurum, Turkey

<sup>c</sup> Department of Physics, College of Science, Princess Nourah Bint Abdulrahman University, P.O. Box 84428, Riyadh, 11671, Saudi Arabia

<sup>d</sup> Department of Medical Diagnostic Imaging, College of Health Sciences, University of Sharjah, 27272, Sharjah, United Arab Emirates

<sup>e</sup> Istinye University, Faculty of Engineering and Natural Sciences, Biomedical Engineering Department, Istanbul, 34396, Turkey

<sup>f</sup> Istinye University, Faculty of Engineering and Natural Sciences, Computer Engineering Department, Istanbul, 34396, Turkey



## ARTICLE INFO

### Keywords:

High entropy alloys  
Refractory-high entropy alloys  
SEM  
EDX  
Gamma-ray  
Neutron

## ABSTRACT

Refractory-High entropy alloys (RHEAs) are known for their exceptional mechanical and radiation-resistant properties, making them promising materials for use in nuclear reactors. Their high entropy composition, which consists of multiple elements in roughly equal proportions, can create a stable microstructure that withstands high levels of radiation damage. The objective of this work is to further our comprehension of the unique behavioral, physical, structural, and nuclear radiation attenuation characteristics shown by High-Entropy Alloys (HEA) and Refractory-High entropy alloy (RHEA) materials. Accordingly, two high entropy alloy (HEA) samples through two different compositions were produced. The first composition under consideration is the typical high-entropy alloy (HEA) defined as MnCrFeNiCoMo0.5. The second composition under consideration is a refractory high entropy alloy (RHEA) characterized by the following elemental composition: TiZrNbHfVTa0.1. SEM and EDX analyses were conducted in terms of determining their physical and structural attributes. Next, a<sup>133</sup>Ba radioisotope together with a HPGe detector were utilized for gamma-ray transmission experiments. Finally, a<sup>241</sup>Am/Be source and a gas proportional detector were used for neutron absorption experiments for HEA and RHEA samples. The alloy structures displayed a unique degree of uniformity. Throughout the RHEA phase, the incorporation of refractory elements did not provide any discernible adverse impacts on the physical stability. The counting spectrum provided a clear explanation of the gamma ray absorption features shown by the RHEA (R) sample, highlighting its exceptional absorption properties. Regarding the absorption properties of neutrons, it was observed that RHEA had a comparatively reduced amount of absorption. Therefore, it can be concluded that the basic structure of RHEA grants it superior gamma-ray attenuation qualities compared to HEA. It can be concluded that RHEA demonstrates superior applicability as a material in comparison to HEA, especially in situations involving the use of fuel rods, where maintaining of neutron quantity has paramount importance for achieving optimum neutron activation.

## 1. Introduction

High-entropy alloys (HEAs) are a currently arose category of materials identified by their particular composition and structure. In contrast to conventional alloys, which commonly comprise one or two predominant elements along with minor quantities of additional alloying elements, HEAs are characterized by the presence of numerous elements in

about equimolar proportions [1–3]. The notion of HEAs was first proposed during the early 2000's and has consequently received considerable attention within the field of materials science and engineering owing to its remarkable attributes and adaptability [1,4–7]. HEAs have drawn considerable interest across several scientific and specific disciplines, including nuclear applications. There are several persuasive motivational factors for the utilization of HEA in the framework of

\* Corresponding author. Department of Medical Diagnostic Imaging, College of Health Sciences, University of Sharjah, 27272, Sharjah, United Arab Emirates.  
E-mail address: [htekint@sharjah.ac.ae](mailto:htekint@sharjah.ac.ae) (H.O. Tekin).

nuclear applications [8–10]. As an instance, the basic structure of HEAs may be modified in order to customize them for certain purposes. The linked versatility of this characteristic enables engineers to come up with materials that have the potential to enhance the efficacy and security of nuclear reactors [11–14]. More importantly, HEAs possessing enhanced thermal conductivity have the potential to provide increased heat transfer efficiency inside reactor components [11,15–17]. HEAs frequently exhibit a synergistic combination of exceptional mechanical characteristics, including elevated tensile strength, flexibility, and hardness [18–20]. The aforementioned characteristics makes them very appropriate for a wide variety of nuclear applications, encompassing from reactor pressure vessels to fuel cladding [13,21,22]. On the contrary, it is well-known that nuclear reactors operate at high temperatures, mandating the materials used in these environments to uphold their structural integrity within extreme circumstances. HEAs frequently exhibit exceptional high-temperature strength and superior resistance to creep, making them appropriate for implementation in high-temperature situations seen in nuclear reactor facilities [23,24]. It is crucial to emphasize that the exposure of materials to ionizing radiation, such as neutrons and gamma rays within nuclear reactors, can lead to their decomposition and degradation over a period. HEAs provide enhanced resistance to radiation-induced damage in comparison to conventional alloys, owing to their distinctive atomic structures and high configurational entropy. The aforementioned characteristic renders HEAs highly appealing for utilization in nuclear reactor components, wherein the utmost importance is placed on the long-term durability and operational efficiency [12,25–28]. Meanwhile, the term refractory-HEA has been presented to the scientific community a while ago. A refractory high-entropy alloy (RHEA) can be categorized as a highly specialized group of HEAs that have been specifically engineered to exhibit exceptional resistance to extremely high temperatures and severe environmental conditions [29,30]. These alloys have been specifically designed to exhibit outstanding thermal resistance and other characteristics that makes them appropriate for implementation in highly demanding environments, particularly in scenarios where conventional materials would prove inadequate [31]. The word refractory within the context of a refractory high-entropy alloy denotes the alloy's inherent ability to endure exceedingly elevated temperatures without experiencing substantial degradation. RHEAs are engineered to retain their structural integrity and mechanical qualities at significantly elevated temperatures, beyond the thermal limits of ordinary materials [32]. Similar to other HEAs, RHEAs consist of numerous constituent elements, often numbering five or more. Each individual element plays a substantial role in determining the collective attributes shown by the alloy as a whole. The selection of these components is carefully done in order to maximize stability at high temperatures and achieve other desirable qualities. Meanwhile, RHEAs are utilized in many industries and sectors characterized by the presence of intense heat and challenging environmental conditions [29,30,33]. Several possible applications encompass aircraft, gas turbine engines, rocket propulsion systems, high-temperature industrial processes, and sophisticated energy systems such as next-generation nuclear reactors [32,34–37]. The field of materials science research is now engaged in the active pursuit of developing and improving refractory high-entropy alloys. Scientists are consistently investigating novel combinations of refractory elements and alloying methodologies in order to fabricate materials that are capable of functioning consistently at higher temperatures and in more rigorous environments. Given the lack of research on RHEA materials and their potential for exceptional performance in extreme conditions, our objective is to undertake a comprehensive study comparing HEA and RHEA materials. This study aims to enhance our understanding of the distinct behavioral, physical, structural, and nuclear radiation attenuation properties exhibited by HEA and RHEA materials. The objective of this study was also to offer an in-depth knowledge of the most suitable conditions for utilizing these materials, hence facilitating informed decision-making by users. The results of this study would provide

valuable insights for researchers interested in examining the differences, behavioral patterns, and attenuation efficiencies between the HEA and RHEA.

## 2. Materials and methods

### 2.1. Experimental procedure for fabrication, physical, and structural properties

In this study, two HEAs samples through two different compositions (see Table 1) were produced (see Fig. 1). The first composition under consideration is the typical high-entropy alloy (HEA) defined as MnCrFeNiCoMo0.5. The second composition under consideration is a refractory high entropy alloy (RHEA) characterized by the following elemental composition: TiZrNbHfVTa0.1. The technique of mechanical alloying (MA) was used to fabricate both HEA and RHEA. The alloy composition was prepared with appropriate proportions and underwent mechanical alloying using a Retsch PM 100 high-energy mill for a period of 100 h. The mechanical alloying (MA) process was performed at a rotating speed of 300 revolutions per minute (rpm), with a ball-to-powder ratio of 20:1. The technique included the use of steel balls of 12 mm in diameter. To mitigate oxidation, the MA treatment procedure was executed under a controlled atmosphere comprising of high-purity argon. During each phase of the milling process, the milling apparatus was programmed to halt its operation for a duration of 30 min after every 30 min of continuous operation. The purpose of using this particular arrangement was to enhance the efficiency of the milling process and mitigate the risk of overheating in the milling vials. We used X-ray diffraction (XRD) technique in terms of performing the microstructural characterization on the HEA and RHEA samples acquired at the end of mechanical alloying process. The X-ray diffraction (XRD) measurements were conducted using a Cu-K $\alpha$  ( $\lambda = 1.54178 \text{ \AA}$ ) radiation source with a voltage of 40 kV and a current of 35 mA. The X-ray Rigaku Miniflex 600 instrument was used for this purpose. The diffraction angle ( $2\theta$ ) spanned from  $10^\circ$  to  $90^\circ$ , with a step size of  $0.02^\circ$ . The evaluation of the material's microstructural morphology was conducted using a scanning electron microscope (SEM; Hitachi-SU3500) equipped with energy dispersive X-ray (EDX) capabilities provided by Oxford-AZtech.

### 2.2. Experimental procedure for gamma-ray and neutron transmission properties

The second phase of experimentation in this research was the examination of the gamma ray and neutron absorption characteristics of the HEA and RHEA samples that were produced. During the first stage of the experimental investigation, the absorption characteristics pertaining to certain gamma energies were ascertained using a High Purity Germanium (HPGe) and the  $^{133}\text{Ba}$  point isotropic radioactive source. Subsequently, the investigation proceeded to the second stage, wherein the absorption characteristics of neutrons with an energy of 4.5 MeV were analyzed. This analysis was conducted using a  $^{241}\text{Am}/\text{Be}$  source with an activity level of 10 mCi. The detection of neutrons emitted by the  $^{241}\text{Am}/\text{Be}$  source and traversing the HEA-RHEA samples was accomplished using a gas proportional-detector, namely the Canberra NP-100B/BF3. Finally, we determined the equivalent absorption dose (EAD) of the HEA and RHEA alloy samples through the equation  $D_0 \cdot D = EAD$ , where EAD is measured in micro sieverts per hour ( $\mu\text{Sv}/\text{h}$ ).

**Table 1**  
Sample codes and elemental structures of HEA and RHEA samples.

Type	Sample Code	Elemental Structure
Refractory High Entropy Alloy (RHEA)	R	TiZrNbHfVTa0.1
High Entropy Alloy (HEA)	G	FeMnCoNiCrMo0.5

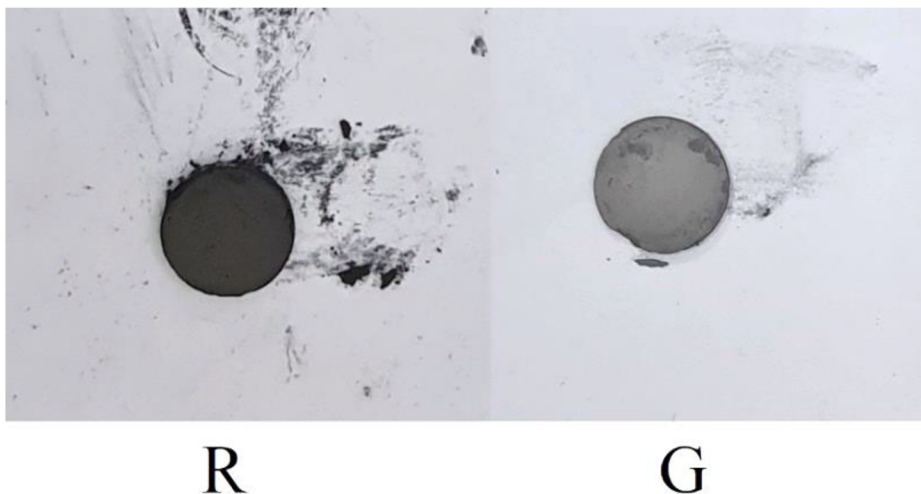


**Fig. 1.** Physical appearances of compacted powders RHEA (R) and HEA (G).

### 3. Results and discussions

#### 3.1. Physical and structural properties of HEA and RHEA samples

XRD spectra of HEA and RHEA samples are given in Fig. 2. In order to see the structural change in the powders, samples were taken from the vials before the MA process was started. These samples, taken before the procedure, are given the name "Raw" in the XRD spectra. In Fig. 2a, the XRD results of the starting powder of the HEA sample and the XRD spectra of the alloy obtained after 100 h of MA treatment are given. Before the MA process, characteristic peaks of the metal powders forming the alloy are observed. After 100 h MA, the peaks belonging to the metals completely disappeared and the characteristic high entropy alloy peaks started to occur, which was between about 42°–44° and at 75°. A similar situation is observed in the RHEA sample (see Fig. 2b). The characteristic metal peaks in the initial powder mixture completely disappeared after MA treatment. Although the structure is amorphous at the end of the MA process, it is seen that there are some recrystallized structures. SEM and EDX results of HEA and RHEA samples are given in Fig. 3. As can be seen in Fig. 3a, at the end of the MA process, the elements that make up the alloy are distributed homogeneously in the structure. At the end of the MA process, powder particles with a spherical shape were obtained. Although the milling agent is used during the MA process, agglomerations have occurred in the powders since there is a long alloying time of 100 h. Due to these agglomerations, the particle size of the alloy powder has in some areas been close to the initial powder size. In Fig. 3b, the results of SEM and EDX analysis of RHEA are given. The MA process has also been successful for producing RHEA. At the end of the MA process, it was observed that the elements forming the alloy were homogeneously distributed in the structure. It can be said that the particle size in the RHEA sample at the end of the MA treatment is smaller than in the HEA sample. Although there is agglomeration in the RHEA sample and the particle size is smaller despite milling for the same time, it can be explained by the elements that make up the alloy. Since the elements that make up RHEA are refractory, less cold welding occurred in this sample. There was less agglomeration in the RHEA sample.

#### 3.2. Gamma-ray attenuation properties of HEA and RHEA samples

In the subsequent part of the study, the gamma ray and absorption properties of samples produced in response to fast neutrons were experimentally evaluated. At first, with a conventional gamma ray transmission configuration (shown in Fig. 4a), the HEA and RHEA samples were positioned between the  $^{133}\text{Ba}$  source and the HPGe

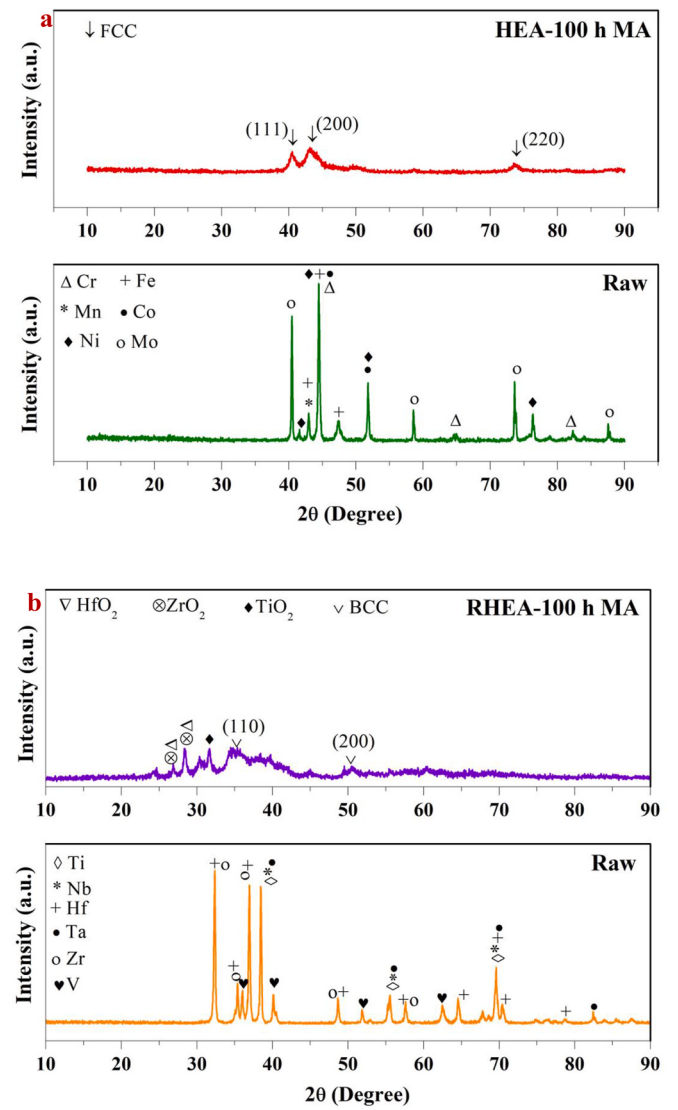
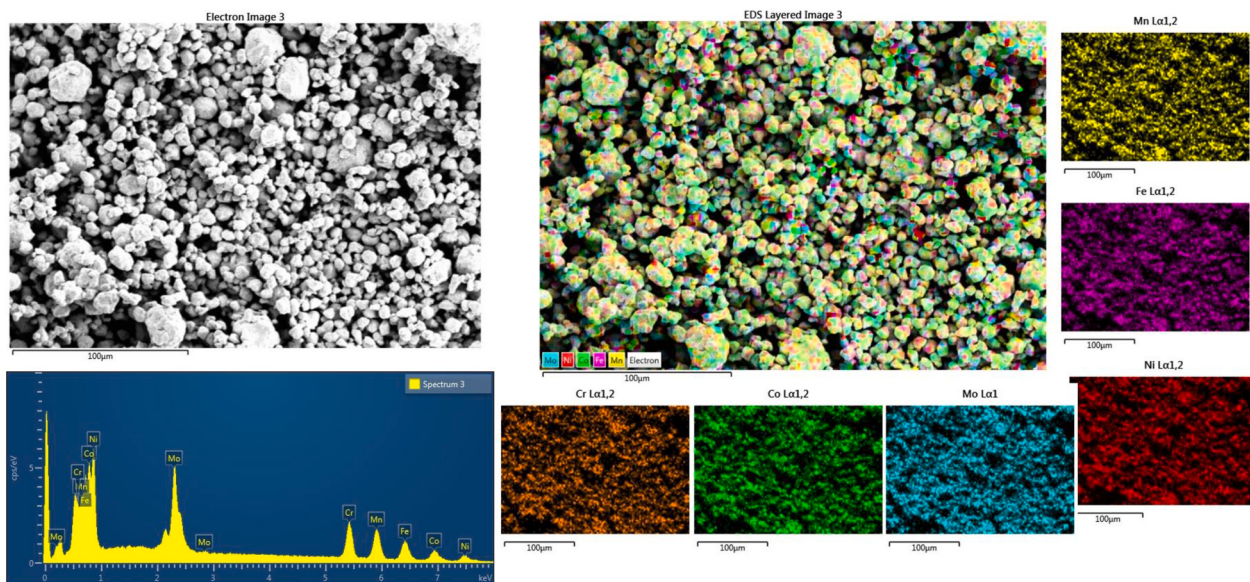
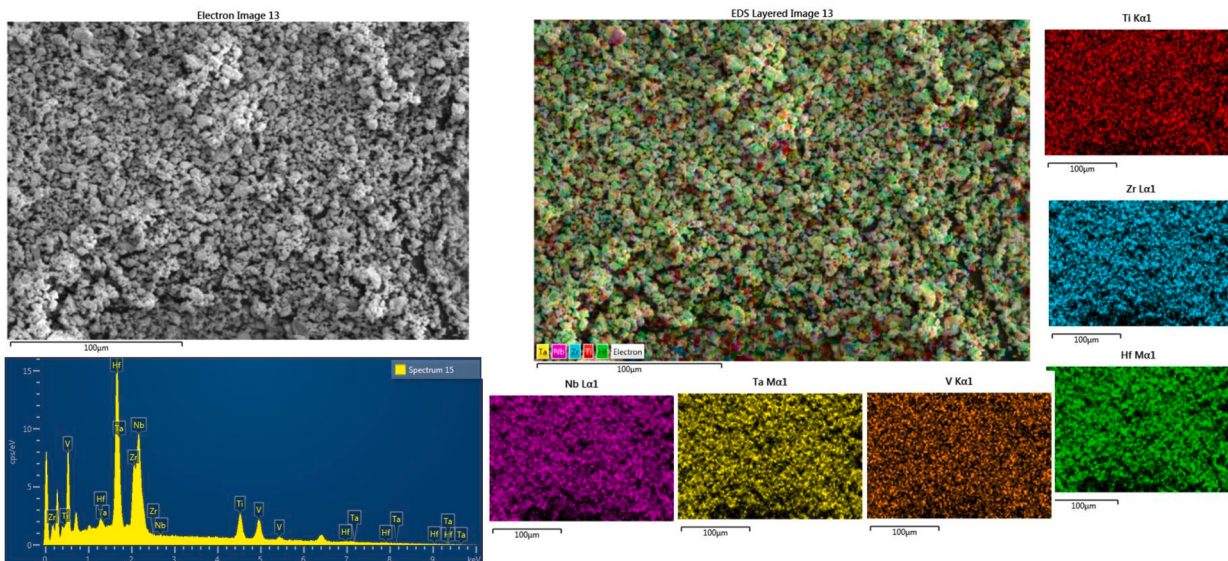


**Fig. 2.** XRD spectra of (a) HEA and (b) RHEA samples.



Element	Ti	Zr	Nb	Hf	V	Ta
Atomic %	22.04	17.83	18.89	18.30	20.56	2.29

(a)



Element	Mn	Cr	Fe	Ni	Co	Mo
Atomic %	17.91	22.85	17.66	17.56	16.87	7.15

(b)

**Fig. 3.** SEM images, EDS-Mapping analyzes and atomic percentages of (a) HEA and (b) RHEA samples.

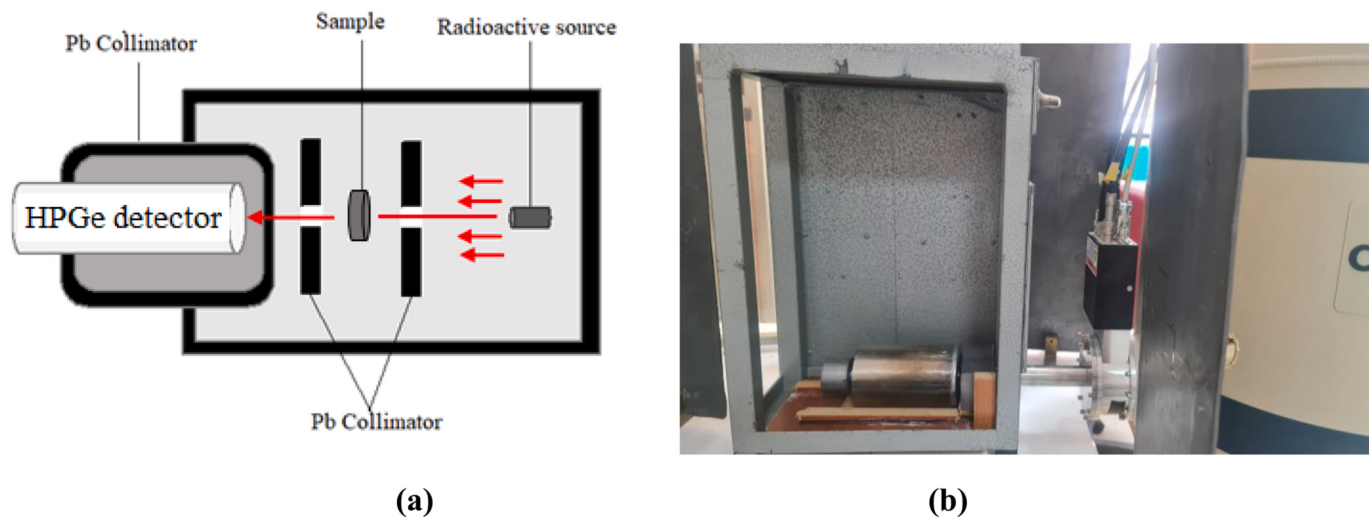


**Fig. 4. (a–b):** (a) Schematic illustration of experimental setup (b) Designed experimental setup for gamma ray transmission measurements for HEA and RHEA samples.

detector, respectively. The HPGe detector was used to measure the secondary gamma rays resulting from the interaction of primary gamma rays emitted by the  $^{133}\text{Ba}$  source, which was surrounded by appropriate Pb blocks (as shown in Fig. 4b), with the HEA (G) and RHEA (R) samples. The data acquired from the detector was analyzed using Maestro software, and the required peak-area analyses were conducted. The absorption spectra obtained from the HPGe detector is shown in Fig. 5 for comparative analysis. The figure illustrates the presence of situations when no absorbing material is placed between the source and the detector, in addition to the R and G samples. The scenario in which there is an absence of absorber material between the detector and the channel is regarded as the circumstance in which the peak values are seen at their highest levels. This phenomenon occurs due to the absence of absorption experienced by the main gamma rays emitted by the source, allowing them to reach the HPGe detector in maximum quantity. However, the count recorded by the HPGe detector exhibited the lowest value for the R sample, while displaying a somewhat higher count for the G sample. The reason for this occurrence is that by positioning the R sample between the source and the HPGe detector, the amount of secondary gamma rays that reach the HPGe detector is minimized, resulting in the highest possible absorption inside the R sample. Likewise, sample G

exhibited absorption; however, the magnitude of absorption in sample G is comparatively lesser than that seen in sample R. Consequently, the secondary gamma rays that traverse the G sample and subsequently reach the HPGe detector exhibit an increased abundance. Upon first examination of the absorption spectra shown in Fig. 5, it becomes apparent that there are obvious differences between the R and G samples. This observation serves as strong proof for the contrasting behaviors exhibited by the high entropy alloy and the refractory high entropy alloy. An attempt was made to provide a more comprehensive understanding of the observed phenomenon by quantifying the absorption coefficients through an analysis of the peak regions shown in Fig. 5. The mass attenuation coefficients (MAC) [38–40] for seven distinct energy values emitted by the  $^{133}\text{Ba}$  were determined by using the related field readings in the given absorption spectrum (see Fig. 5). Following the completion of these calculations, the experimental outcomes were then compared to the theoretical mass attenuation coefficients (MAC) values derived for the corresponding compositions using the EpiXS code. Fig. 6 illustrates the variations in MAC values for the R and G sample as a function of energy, in contrast to the MAC values achieved through the EpiXS [41] code (see Table 2). The figure illustrates that the MAC value

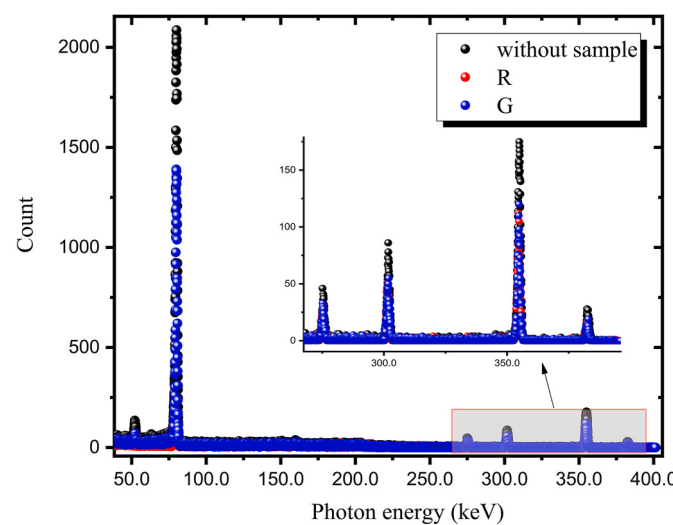


**Fig. 5.** Absorption spectra of HEA and RHEA samples obtained through  $^{133}\text{Ba}$  radioactive source.

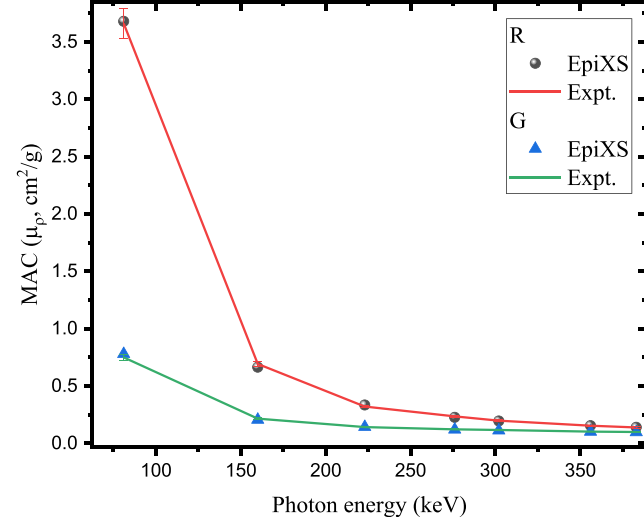


**Fig. 6.** Variation of mass attenuation coefficients (MAC) against photon energy for RHEA and HEA samples.

**Table 2**

Experimental and theoretical mass attenuation coefficients ( $\mu_p$ ,  $\text{cm}^2/\text{g}$ ) for the R and G samples.

Energy (keV)	R			G		
	EpiXS	Expt.	Error	EpiXS	Expt.	Error
81	3.6804	3.6612	0.1281	0.7791	0.7499	0.0263
160	0.6641	0.6932	0.0243	0.2064	0.2163	0.0076
223	0.3352	0.3215	0.0113	0.1438	0.1420	0.0050
276	0.2272	0.2358	0.0083	0.1206	0.1225	0.0043
302	0.1954	0.1981	0.0069	0.1130	0.1174	0.0041
356	0.1547	0.1545	0.0054	0.1019	0.1034	0.0036
383	0.1403	0.1389	0.0049	0.0975	0.0996	0.0035

of 81 keV yielded the lowest result. The MAC values of both the R and G samples exhibited a declining pattern as a result of the rise in energy. The observed phenomenon corresponds to the reduction in the rate at which gamma rays are attenuated inside a substance as a consequence of an increase in the energy level of gamma rays. Stated alternatively, the increase in energy levels resulted in enhanced penetration capabilities while simultaneously decreasing the probability of absorption inside the material. The MAC values obtained for the R sample had higher values at each energy level, displaying significant differences when compared to the G sample. The observed difference is well-known, particularly when considering lower energy levels. Based on the results, the addition of refractory characteristics to high entropy alloys resulted in significant enhancements in both their structural characteristics and their capacity for gamma ray absorption. The aforementioned result is a significant finding that confirms the higher absorption capabilities of RHEAs in comparison to HEAs. A further critical analysis was conducted to compare RHEA and HEA in terms of their HVL [42–45] values. The HVL value of a material refers to the minimum thickness of the material necessary to reduce the intensity of the primary gamma ray by half upon interaction. Superior gamma ray absorption characteristics are correlated with a low HVL values. Fig. 7 presents a comparative analysis of the HVL values for several alloys that have been previously examined in the literature, together with the R and G samples. The figure illustrates a consistent upward trend in HVL values across all alloys, corresponding to an increase in energy. The main reason for requiring thicker materials to effectively attenuate high-energy gamma rays is of utmost significance. The obtained HVL values for RHEA exhibit a significant decrease in comparison to the values obtained for HEA. This suggests that RHEA offers a benefit not just over HEA, but also over other alloys often used in

nuclear applications, such as FeCoNiMnCr [46], REX-734 [47], 316L-SS [47], S3 [48] samples. As an example, the HVL results acquired for RHEA at an energy level of 223 keV show a nearly three-fold decrease compared to the same value observed for HEA. This demonstrates that the use of RHEA may result in a reduction of almost thrice in the thickness of the alloy required to attenuate the amount of 223 keV gamma rays by half. Furthermore, using RHEA enables the achievement of the same attenuation effect even when the thickness is reduced by a factor of three. The parameter known as Exposure Buildup Factor (EBF) has significant importance within the domain of nuclear engineering and radiation shielding. This parameter is used for the evaluation of material behavior under the influence of ionizing radiation, including gamma rays and X-rays. EBF has substantial importance in the design and assessment of radiation shielding materials for nuclear reactors and other facilities that release radiation [49–53]. Basically, EBF is a quantitative indicator of the extent to which radiation exposure, or simply exposure, intensifies in relation to the thickness of a certain material. On the other hand, EBF considers the occurrence of several scattering and absorption events inside the material. In the context of nuclear reactor applications, an in-depth knowledge of the EBF of materials hold significant importance in the optimization of shielding design. This understanding helps in the determination of the extent to which the shielding material absorbs energy, thereby playing a critical role in the mitigation of secondary radiation, such as scatter. Fig. 8a and b depict the behavior of energy absorption buildup factor (EABF) values across different energy zones. Both R and G samples show a sharp increase in EABF values, peaking at around 0.01–0.02 MeV. This peak is especially prominent in the R sample. The sharp peak suggests that both materials have a significant photoelectric absorption in this energy range. This is typical for many materials where the photoelectric effect is dominant at low energies. The EABF values for both samples decrease in this zone, with the R sample showing a more pronounced dip. This zone is dominated by Compton scattering. The decrease implies that fewer scattered photons are absorbed in the material. In the high energy region, the EABF values plateau and exhibits a wavy behavior for both samples. The values for the R sample are generally lower than those for the G sample across varying mean free paths. The plateauing suggests a balance between incoming and outgoing scattered photons, implying less variation in energy absorption. Fig. 9 depicts the variation of exposure buildup factors (EBF) against photon energy at different penetration depths for (a) RHEA (b) HEA samples. As the energy of gamma rays rises, there is a general tendency for the EBF to decrease. This implies that gamma rays with higher energy possess more penetration capabilities and need a smaller amount of supplementary shielding material in order to decrease their intensity to a specified level. The correlation between EBF and gamma ray energy is often characterized by an exponential relationship. This implies that even little increases in energy may lead to substantial decreases in EBF values. Based on Figs. 8 and 9, we can observe the behavior of the EABF and EBF for R and G against photon energy, and as stated, the G has a higher EABF value around 1 MeV compared to the R. The difference in the EABF and EABF values between the two materials can be attributed to several factors. The inherent atomic composition of the two materials plays a vital role. Materials with higher atomic numbers tend to have higher photon interaction probabilities. Around the energy range of 1 MeV, Compton scattering is a predominant interaction mechanism. However, the onset of pair production might also start to contribute. The density of the material can also influence the buildup factor. A denser material will generally have a higher number of atoms per unit volume, which can increase the likelihood of photon interactions and thus can change the buildup factor values. Another reason for this phenomenon can be attributed to the microstructure, grain boundaries, and other structural factors that can also influence photon interaction probabilities. In essence, the higher EABF value for G around 1 MeV compared to R can be attributed to the intrinsic material properties and composition of the high entropy alloys. Fig. 10 illustrates the variation in EBF values at different penetration depths for both

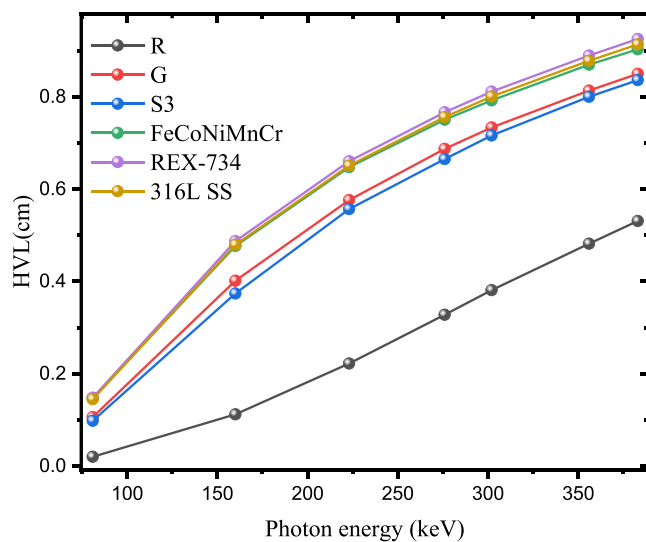
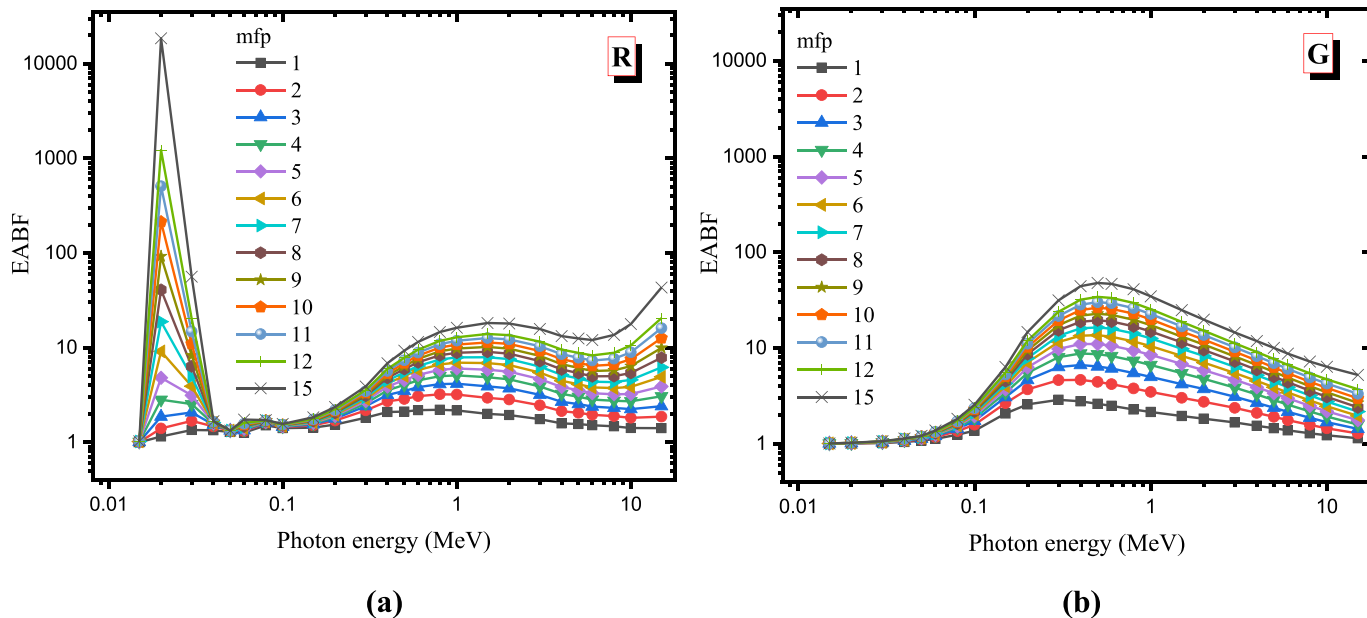
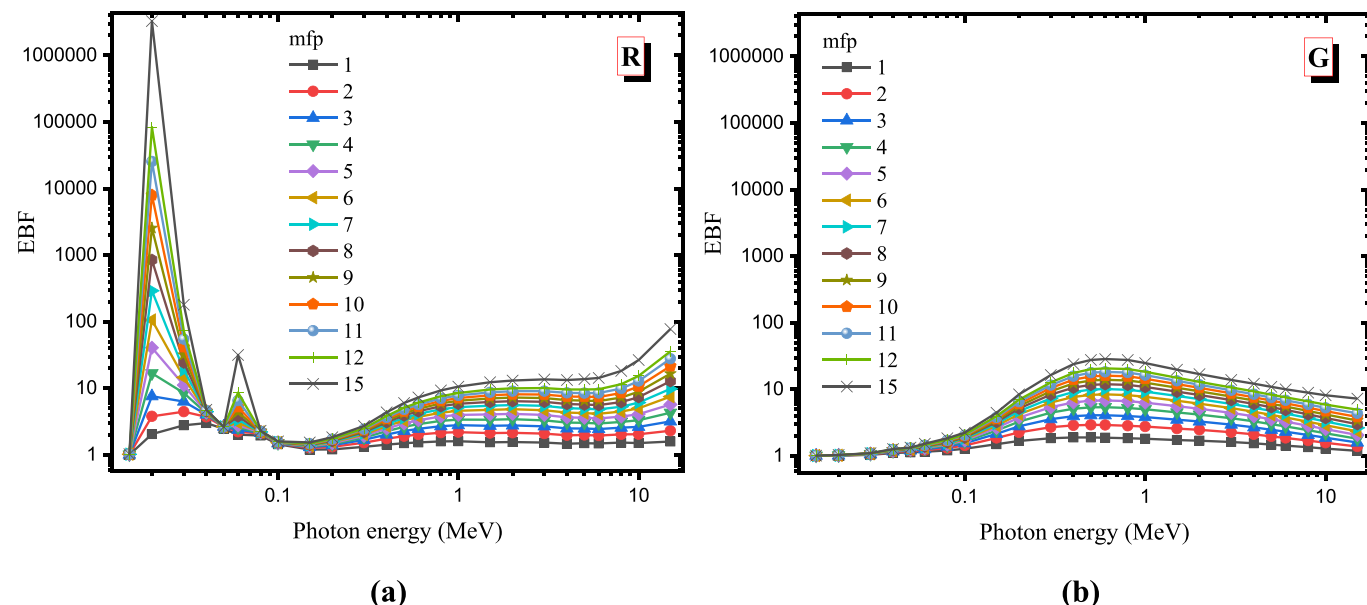


Fig. 7. Comparison of half value layer (HVL) values for R, G and other alloys such as FeCoNiMnCr [46], REX-734 [47], 316L-SS [47], S3 [48] samples.



**Fig. 8.** Variation of energy absorption buildup factors (EABF) for (a) RHEA (b) HEA samples against photon energy at different penetration depths from 1 mfp to 15 mfp.



**Fig. 9.** Variation of exposure buildup factors (EBF) for (a) RHEA (b) HEA samples against photon energy at different penetration depths from 1 mfp to 15 mfp.

RHEA and HEA samples, while maintaining a constant photon energy of 0.5 MeV. The data reveals that the RHEA (R) sample exhibits lower EBF values in comparison to HEA (G), indicating a potential advantage in gamma-ray attenuation. Therefore, it may be suggested that the basic structure of RHEA grants it superior gamma-ray attenuation qualities compared to HEA.

### 3.3. Neutron attenuation properties of HEA and RHEA samples

The investigation of neutron absorption characteristics in various materials, such as high entropy alloys (HEAs), has significant significance in the field of nuclear applications, namely in the domain of nuclear reactor design and development. The characteristics related to the absorption of neutrons are of utmost importance in ensuring the safety,

effectiveness, and functionality of these systems. Nuclear reactors release a range of radiation types, which include neutrons among others. The use of neutron shielding materials is essential in order to protect workers, equipment, and the surrounding ecosystem from undue levels of neutron radiation. HEAs that possess customized neutron absorption qualities have the potential to serve as efficient neutron shields, therefore mitigating radiation exposure. The process of neutron absorption plays a crucial role in the regulation of neutron flux inside a nuclear reactor. In order to maintain and regulate the nuclear chain reaction, reactors need a careful equilibrium between neutron absorption and moderation. Strategically positioning materials with distinct neutron absorption capabilities inside a reactor enables the regulation of neutron flux and the maintenance of the reactor at the intended power level. This work also included the determination of neutron absorption parameters

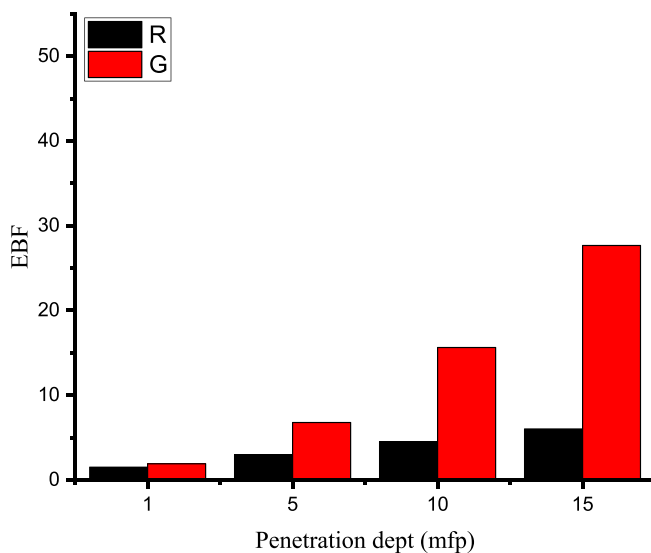


Fig. 10. Variation of (a) EABF and (b) EBF values in several penetration depths for HEA and RHEA samples at fixed 0.5 MeV photon energy.



Fig. 11. Utilized experimental setup for fast neutron dose measurements through  $^{241}\text{Am}/\text{Be}$  neutron source.

of HEA and RHEA using  $\alpha^{241}\text{Am}/\text{Be}$  source and a gas proportional detector (see Fig. 11). The experimental findings of neutron dose measurements for the HEA and RHEA samples are shown in Table 3. As seen, the measured equivalent dose rate in the absence of the sample is 1.511  $\mu\text{Sv}/\text{h}$ . However, the placement of the R sample results in a drop in the equivalent dose rate from 1.511  $\mu\text{Sv}/\text{h}$  to 0.676  $\mu\text{Sv}/\text{h}$ . Yet, the aforementioned value noticed an increase from 0.676  $\mu\text{Sv}/\text{h}$  to 0.914  $\mu\text{Sv}/\text{h}$  as a result of the replacement of R with G. In contrast, RHEA has shown an absorption rate of 44.73% for the initial neutron dose, whereas HEA has exhibited an absorption rate of 60.48% for the administered neutron dose. The experimental results have been validated by calculating the effective removal cross section ( $\Sigma_R$ ) of the RHEA (R) and HEA (G) samples, as seen in Fig. 12. The same relationship between the R and G

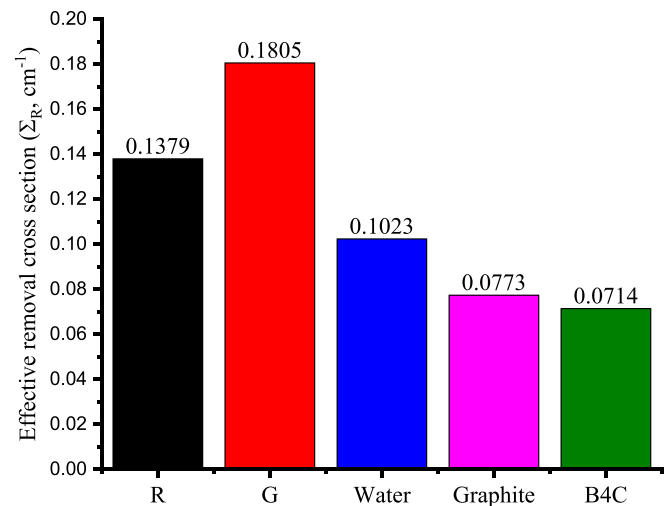


Fig. 12. Comparison of effective removal cross section ( $\Sigma_R$ ) values between HEA, RHEA, and other well-known neutron absorbers such as Water, Graphite and  $\text{B}_4\text{C}$ .

samples was also seen for the total of R values. Hence, it can be said that RHEA (R) exhibits comparatively reduced neutron absorption characteristics in comparison to HEA (G). The finding made in this research may be regarded as very significant. This is due to the fact that some components of nuclear reactors need possess reduced neutron absorption qualities when used as fuel rod material, in order to maintain neutron activation within acceptable limits.

#### 4. Conclusion

The main goal of this work was to investigate the vital changes in behaviour that arise in the material during the transition from high entropy alloys to refractory high entropy alloys. Given that these materials are the primary substances used in nuclear reactors, it is of utmost importance to comprehend the variations that may arise in the absorption qualities of gamma rays and neutrons throughout a period of transformation. Classical high-entropy alloys (HEAs) are composed of transition metals, namely iron (Fe), nickel (Ni), chromium (Cr), manganese (Mn), and cobalt (Co). The cost of producing high-entropy alloys (HEA) is reduced due to the comparatively low costs of these metals. Classical high-entropy alloys (HEAs) were characterized by either a body-centred cubic (BCC) or face-centred cubic (FCC) crystal structure. In contrast, refractory high-entropy alloys RHEAs consist of pricier metallic elements with refractory properties, including Zirconium (Zr), Tungsten (W), Hafnium (Hf), and Tantalum (Ta). RHEAs have a body-centred cubic (BCC) crystal structure. While classical HEAs exhibit superior performance compared to ordinary alloys, it is noteworthy that the performance of RHEAs surpasses that of classical HEAs in high-temperature applications. Furthermore, several characteristics of room temperature RHEAs exhibit superiority over conventional HEAs. Considering the situations in which two materials with FCC and BCC crystal structures are exposed to irradiation by heavy, energetic particles, it has been revealed that the structural change caused by irradiation is less in the BCC structured material [54]. From this perspective, RHEAs are a more suitable material group for radiation applications. However, in addition to parameters such as high temperature resistance and resistance to radiation damage, another important feature expected from the material in nuclear reactor applications is radiation shielding. In this study, the radiation shielding properties of HEAs and RHEAs, beyond their known properties (such; high temperature resistance, oxidation, creep behavior), were compared. For this purpose, a classical HEA and RHEA were produced under the same conditions. According to

Table 3  
Experimental results of neutron dose measurements for the R and G samples.

Sample	Equivalent Dose Rates Absorbed by Samples ( $\mu\text{Sv}/\text{h}$ )	Absorbed Dose Rate (%)
Do	1.511	—
R	0.676	44.73
G	0.914	60.48

- The alloy structures exhibited a unique level of homogeneity.
- During the RHEA phase, the introduction of refractory materials did not result in any detectable detrimental effects on the physical structure.
- The gamma ray absorption characteristics of the RHEA (R) sample were clearly explained in the counting spectrum, demonstrating superior absorption attributes.
- In instances when materials of the HEA (High Entropy Alloy) and RHEA (Refractory High Entropy Alloy) categories are used as components in nuclear reactors, the inclusion of refractories can be recognized as a viable approach for scenarios where there is a need for materials with high gamma absorption qualities.
- At HVL values, RHEA exhibits an absorption process that is roughly three times more efficient than HEA.
- Consequently, RHEA occupies less physical space while offering enhanced utilization area efficiency.
- In relation to neutron absorption characteristics, RHEA exhibited a lower level of absorption. Based on the evidence presented, it can be inferred that RHEA exhibits greater suitability as a material compared to HEA, particularly in scenarios involving the use of fuel rods where the maintaining of neutron quantity is of the utmost significance for optimal neutron activation.

The findings resulted from this research included a pioneering investigation that conducted a thorough comparative analysis of refractory high entropy alloys and high entropy alloys with respect to their absorption and physical characteristics. It is important to conclude that more research is required for the integration of other refractory components. By conducting further examinations, researchers could acquire a deeper understanding of both the extent to which refractory components contribute to important attributes and the specific refractory element that provides the most effective contributions.

## Funding

None

## Data availability statement

Data available on request from the authors.

## Author contributions

Conceptualization: Seval Hale Guler, Omer Guler, Huseyin Ozan Tekin, Bashar Issa; Methodology: Omer Guler, Huseyin Ozan Tekin, Esra Kavaz; Formal analysis and investigation: Ghada ALMisned, Seval Hale Guler, Esra Kavaz, Omer Guler; Writing - original draft preparation: Omer Guler, Huseyin Ozan Tekin; Writing - review and editing: Omer Guler, Huseyin Ozan Tekin, Bashar Issa, Ghada ALMisned; Supervision: Huseyin Ozan Tekin, Omer Guler.

## Declaration of competing interest

The authors declare that they have no known competing financial interests or personal relationships that could have appeared to influence the work reported in this paper.

## Acknowledgement

The authors would like to thank Münzur University (Project no. MFMUB023-01) for the financial support during the studies.

## References

- [1] J.W. Yeh, S.K. Chen, S.J. Lin, J.Y. Gan, T.S. Chin, T.T. Shun, C.H. Tsau, S.Y. Chang, Nanostructured high-entropy alloys with multiple principal elements: novel alloy design concepts and outcomes, *Adv. Eng. Mater.* 6 (2004) 299–303.
- [2] J.-W. Yeh, Overview of high-entropy alloys, *High-entropy alloys: fundamentals and applications* (2016) 1–19.
- [3] S.H. Güler, The effect of using ferro-alloy on the properties of AlCoFeNiMoTi high-entropy alloy produced by arc-melting method: design of low cost, *Int. J. Metalcast.* (2023) 1–10.
- [4] E.P. George, D. Raabe, R.O. Ritchie, High-entropy alloys, *Nat. Rev. Mater.* 4 (2019) 515–534.
- [5] M.-H. Tsai, J.-W. Yeh, High-entropy alloys: a critical review, *Materials Research Letters* 2 (2014) 107–123.
- [6] Y. Ye, Q. Wang, J. Lu, C. Liu, Y. Yang, High-entropy alloy: challenges and prospects, *Mater. Today* 19 (2016) 349–362.
- [7] Y. Zhang, T.T. Zuo, Z. Tang, M.C. Gao, K.A. Dahmen, P.K. Liaw, Z.P. Lu, Microstructures and properties of high-entropy alloys, *Prog. Mater. Sci.* 61 (2014) 1–93.
- [8] E.J. Pickering, A.W. Carruthers, P.J. Barron, S.C. Middleburgh, D.E. Armstrong, A. S. Gandy, High-entropy alloys for advanced nuclear applications, *Entropy* 23 (2021) 98.
- [9] P. Barron, A. Carruthers, J. Fellowes, N. Jones, H. Dawson, E. Pickering, Towards V-based high-entropy alloys for nuclear fusion applications, *Scripta Mater.* 176 (2020) 12–16.
- [10] A. Kaireer, J. Waite, B. Li, A. Couet, D. Armstrong, A. Wilkinson, Low activation, refractory, high entropy alloys for nuclear applications, *J. Nucl. Mater.* 526 (2019), 151744.
- [11] M. Moschetti, P.A. Burr, E. Obbard, J.J. Kruzic, P. Hosemann, B. Gludovatz, Design considerations for high entropy alloys in advanced nuclear applications, *J. Nucl. Mater.* 567 (2022), 153814.
- [12] S.-q. Xia, W. Zhen, T.-f. Yang, Y. Zhang, Irradiation behavior in high entropy alloys, *J. Iron Steel Res. Int.* 22 (2015) 879–884.
- [13] T. Shi, P.-H. Lei, X. Yan, J. Li, Y.-D. Zhou, Y.-P. Wang, Z.-X. Su, Y.-K. Dou, X.-F. He, D. Yun, Current development of body-centered cubic high-entropy alloys for nuclear applications, *Tungsten* 3 (2021) 197–217.
- [14] Y. Lu, H. Huang, X. Gao, C. Ren, J. Gao, H. Zhang, S. Zheng, Q. Jin, Y. Zhao, C. Lu, A promising new class of irradiation tolerant materials: Ti2ZrHfV0.5Mo0.2 high-entropy alloy, *J. Mater. Sci. Technol.* 35 (2019) 369–373.
- [15] S. Xia, M.C. Gao, T. Yang, P.K. Liaw, Y. Zhang, Phase stability and microstructures of high entropy alloys ion irradiated to high doses, *J. Nucl. Mater.* 480 (2016) 100–108.
- [16] Y. Zong, N. Hashimoto, H. Oka, Study on irradiation effects of refractory bcc high-entropy alloy, *Nuclear Materials and Energy* 31 (2022), 101158.
- [17] X. Wang, H. Huang, J. Shi, H.-Y. Xu, D.-Q. Meng, Recent progress of tungsten-based high-entropy alloys in nuclear fusion, *Tungsten* 3 (2021) 143–160.
- [18] W. Zhang, A. Chabok, B.J. Kooi, Y. Pei, Additive manufactured high entropy alloys: a review of the microstructure and properties, *Mater. Des.* 220 (2022), 110875.
- [19] Z.U. Arif, M.Y. Khalid, E. ur Rehman, Laser-aided additive manufacturing of high entropy alloys: processes, properties, and emerging applications, *J. Manuf. Process.* 78 (2022) 131–171.
- [20] C. Zhu, L. Xu, M. Liu, M. Guo, S. Wei, A review on improving mechanical properties of high entropy alloy: interstitial atom doping, *J. Mater. Res. Technol.* 24 (2023) 7832–7851.
- [21] P. Ferreira, S. von Tiedemann, N. Parkes, D. Gurah, D. King, P. Norman, M. Gilbert, A. Knowles, VNbCrMo refractory high-entropy alloy for nuclear applications, *Int. J. Refract. Metals Hard Mater.* 113 (2023), 106200.
- [22] A. Ayyagari, R. Salloom, S. Muskeri, S. Mukherjee, Low activation high entropy alloys for next generation nuclear applications, *Materialia* 4 (2018) 99–103.
- [23] Z. Cheng, J. Sun, X. Gao, Y. Wang, J. Cui, T. Wang, H. Chang, Irradiation effects in high-entropy alloys and their applications, *J. Alloys Compd.* 930 (2023), 166768.
- [24] D. King, S. Cheung, S.A. Humphry-Baker, C. Parkin, A. Couet, M. Cortie, G. Lumpkin, S. Middleburgh, A.J. Knowles, High temperature, low neutron cross-section high-entropy alloys in the Nb-Ti-V-Zr system, *Acta Mater.* 166 (2019) 435–446.
- [25] T. Egami, W. Guo, P. Rack, T. Nagase, Irradiation resistance of multicomponent alloys, *Metall. Mater. Trans.* 45 (2014) 180–183.
- [26] D. Patel, M.D. Richardson, B. Jim, S. Akhmadaliev, R. Goodall, A.S. Gandy, Radiation damage tolerance of a novel metastable refractory high entropy alloy V2.5Cr1.2WMoCo0.04, *J. Nucl. Mater.* 531 (2020), 152005.
- [27] S. Xia, X. Yang, T. Yang, S. Liu, Y. Zhang, Irradiation resistance in Al x CoCrFeNi high entropy alloys, *Jom* 67 (2015) 2340–2344.
- [28] C. Lu, L. Niu, N. Chen, K. Jin, T. Yang, P. Xiu, Y. Zhang, F. Gao, H. Bei, S. Shi, Enhancing radiation tolerance by controlling defect mobility and migration pathways in multicomponent single-phase alloys, *Nat. Commun.* 7 (2016), 13564.
- [29] O. Senkov, G. Wilks, D. Miracle, C. Chuang, P. Liaw, Refractory high-entropy alloys, *Intermetallics* 18 (2010) 1758–1765.
- [30] J.-l. Zhou, Y.-h. Cheng, Y.-x. Chen, X.-b. Liang, Composition design and preparation process of refractory high-entropy alloys: a review, *Int. J. Refract. Metals Hard Mater.* 105 (2022), 105836.
- [31] M. Gao, C. Carney, Ö. Doğan, P. Jablonksi, J. Hawk, D. Alman, Design of refractory high-entropy alloys, *Jom* 67 (2015) 2653–2669.
- [32] W. Xiong, A.X. Guo, S. Zhan, C.-T. Liu, J.-W. Yeh, S.C. Cao, Refractory high-entropy alloys: a focused review of preparation methods and properties, *J. Mater. Sci. Technol.* 142 (2022) 196–215.

- [33] M. Srikanth, A.R. Annamalai, A. Muthuchamy, C.-P. Jen, A review of the latest developments in the field of refractory high-entropy alloys, *Crystals* 11 (2021) 612.
- [34] X. Ren, Y. Li, Y. Qi, B. Wang, Review on preparation technology and properties of refractory high entropy alloys, *Materials* 15 (2022) 2931.
- [35] S. Chen, C. Qi, J. Liu, J. Zhang, Y. Wu, Recent advances in W-containing refractory high-entropy alloys—an overview, *Entropy* 24 (2022) 1553.
- [36] S. Dixit, S. Rodriguez, M.R. Jones, P. Buzby, R. Dixit, N. Argibay, F.W. DelRio, H. H. Lim, D. Fleming, Refractory high-entropy alloy coatings for high-temperature aerospace and energy applications, *J. Therm. Spray Technol.* 31 (2022) 1021–1031.
- [37] X.-J. Hua, P. Hu, H.-R. Xing, J.-Y. Han, S.-W. Ge, S.-L. Li, C.-J. He, K.-S. Wang, C.-J. Cui, Development and property tuning of refractory high-entropy alloys: a review, *Acta Metall. Sin.* 35 (2022) 1231–1265.
- [38] N. Demir, U.A. Tarim, M.A. Popovici, et al., Investigation of mass attenuation coefficients of water, concrete and bakelite at different energies using the FLUKA Monte Carlo code, *J. Radioanal. Nucl. Chem.* 298 (2013) 1303–1307, <https://doi.org/10.1007/s10967-013-2494-y>.
- [39] I. Akkurt, C. Basyigit, S. Kilincarslan, B. Mavi, A. Akkurt, Radiation shielding of concretes containing different aggregates, *Cement Concr. Compos.* 28 (2) (2006) 153–157, <https://doi.org/10.1016/j.cemconcomp.2005.09.006>.
- [40] Rajnish Kaur, Anil Kumar, Janos Osan, M. Czyzicki, A.G. Karydas, Sanjiv Puri, Measurements of mass attenuation coefficients and determination of photoionization cross sections at energies across the Li ( $i=1-3$ ) edges of 66Dy, *Radiat. Phys. Chem.* 136 (2017) 30–37, <https://doi.org/10.1016/j.radphyschem.2017.03.028>.
- [41] Frederick C. Hila, Alvie Asuncion-Astronomo, Cheri Anne M. Dingle, Julius Federico M. Jecong, Abigale Mia V. Javier-Hila, Mon Bryan Z. Gili, Charlotte V. Balderas, Girlie Eunice P. Lopez, Neil Raymond D. Guillermo, Alberto V. Amorsolo, EpiXS: a Windows-based program for photon attenuation, dosimetry and shielding based on EPICS2017 (ENDF/B-VIII) and EPDL97 (ENDF/B-VI.8), *Radiat. Phys. Chem.* 182 (2021), 109331, <https://doi.org/10.1016/j.radphyschem.2020.109331>.
- [42] H.O. Tekin, Ghada Almisned, Shams A.M. Issa, Hesham M.H. Zakaly, A rapid and direct method for half value layer calculations for nuclear safety studies using MCNPX Monte Carlo code, *Nucl. Eng. Technol.* 54 (2022) 9, <https://doi.org/10.1016/j.net.2022.03.037>.
- [43] G. Lakshminarayana, H.O. Tekin, M.G. Dong, M.S. Al-Buraihi, Dong-Eun Lee, Jonghun Yoon, Taejoon Park, Comparative assessment of fast and thermal neutrons and gamma radiation protection qualities combined with mechanical factors of different borate-based glass systems, *Results Phys.* 37 (2022), 105527, <https://doi.org/10.1016/j.rinp.2022.105527>.
- [44] Ghada Almisned, Exploring a monotonically non-decreasing behavioral function on shielding properties and transmission factors in borosilicate glasses through heavy metal oxide reinforcement, *Radiat. Phys. Chem.* 111262 (2023), <https://doi.org/10.1016/j.radphyschem.2023.111262>. ISSN 0969-806X.
- [45] Ghada Almisned, Duygu Sen Baykal, Erkan Ilik, Mohammed Abuzaid, A. Shams, M. Issa, Gokhan Kilic, M. Hesham, H. Zakaly, Antoaneta Ene, Huseyin Ozan Tekin, Tungsten (VI) oxide reinforced antimony glasses for radiation safety applications: a throughout investigation for determination of radiation shielding properties and transmission factors, *Heliyon* (2023), e17838, <https://doi.org/10.1016/j.heliyon.2023.e17838>.
- [46] Telem Şimşek, Esra Kavaz, Ömer Güler, Tuncay Şimşek, Barış Avar, Naim Aslan, Ghada Almisned, Hesham M.H. Zakaly, H.O. Tekin, FeCoNiMnCr high-entropy alloys (HEAs): synthesis, structural, magnetic and nuclear radiation absorption properties, *Ceram. Int.* 49 (15) (2023) 25364–25370, <https://doi.org/10.1016/j.ceramint.2023.05.072>. ISSN 0272-8842.
- [47] Y. Say, Ö. Güler, E. Kavaz, G. Almisned, A. Ene, H.O. Tekin, Structural, physical, and radiation absorption properties of a significant nuclear power plant component: a comparison between REX-734 and 316L SS austenitic stainless steels, *Open Chem.* 21 (2023), 20220307.
- [48] Ömer Güler, E. Kavaz, Seval Hale Güler, Ghada Almisned, İskender Özkul, Öyküm Basgoz, H.O. Tekin, Oxides dispersion-strengthened (ODS) FeCoNiCuZn high entropy alloys through different rare earth elements: synthesis, structural, physical, and experimental radiation transmission properties, Part A, *Ceram. Int.* 49 (22) (2023) 35021–35033, <https://doi.org/10.1016/j.ceramint.2023.08.176>. ISSN 0272-8842.
- [49] M.I. Sayyed, M.Y. Al-Zaatreh, M.G. Dong, M.H.M. Zaid, K.A. Matori, H.O. Tekin, A comprehensive study of the energy absorption and exposure buildup factors of different bricks for gamma-rays shielding, *Results Phys.* 7 (2017) 2528–2533, <https://doi.org/10.1016/j.rinp.2017.07.028>.
- [50] H.O. Ozge Kilicoglu, Tekin, Bioactive glasses with  $TiO_2$  additive: behavior characterization against nuclearradiation and determination of buildup factors, *Ceram. Int.* 46 (2020) 10779–10787, <https://doi.org/10.1016/j.ceramint.2020.01.088>.
- [51] Ghada Almisned, Duygu Sen Baykal, Fatema T. Ali, Ghaida Bilal, G. Kilic, H. O. Tekin, Gadolinium-tungsten-boron trioxide glasses: a multi-phase research on cross-sections, attenuation coefficients, build-up factors and individual transmission factors using MCNPX, *Optik* 272 (2022), 170216, <https://doi.org/10.1016/j.ijleo.2022.170216>.
- [52] Yonca Yahsi Celen, Mucize Saruhan, Ghada Almisned, Huseyin Ozan Tekin, Ekmekeci Ismail, Calculation of gamma-ray buildup factors for some medical materials, *Emerg. Mater. Res.* 11 (3) (2022) 388–398, <https://doi.org/10.1680/jemmr.22.00051>.
- [53] Ghada Almisned, Duygu Sen Baykal, E. Ilik, Mohammed Abuzaid, Gokhan Kilic, H. O. Tekin, Functional assessment of various rare-earth (RE) ion types: an investigation on gamma-ray attenuation properties of  $GeO_2\text{-}B_2O_3\text{-}P_2O_5\text{-}ZnO\text{-}Tb_2O_3\text{-}RE$  magneto-optical glasses, *Optik* 274 (2023), 170526, <https://doi.org/10.1016/j.ijleo.2023.170526>.
- [54] S.J. Zinkle, Fusion materials science: overview of challenges and recent progress, *Phys. Plasmas* 12 (2005), 058101, <https://doi.org/10.1063/1.1880013>.